

Structured illumination for the extension of imaging interferometric microscopy

Alexander Neumann,* Yuliya Kuznetsova, and S. R. J. Brueck

Center for High Technology Materials and Departments of Physics and Astronomy and Electrical and Computer Engineering, University of New Mexico, 1313 Goddard SE, Albuquerque, New Mexico, USA

*Corresponding author: aneumann@chtm.unm.edu

Abstract: Structured illumination applied to imaging interferometric microscopy (IIM) allows extension of the resolution limit of low numerical aperture objective lenses to ultimate linear systems limits ($\lesssim \lambda/4$ in air) without requiring a reference beam around the objective lens. Instead, the reference beam is provided by an illumination beam just at the edge of the optical system numerical aperture resulting in a shift of the recorded spatial frequencies (equivalent to an intermediate frequency). The restoration procedure is discussed. This technique is adaptable readily to existing microscopes, since extensive access to the imaging system pupil plane is not required.

©2008 Optical Society of America

OCIS codes: (190.0190) Microscopy; (110.3175) Interferometric imaging.

References and links

1. E. Abbe, Arch. Mikrosk. Anat. Entwicklungsmech. **9**, 413 – 420 (1873).
2. M. G. L. Gustafsson, "Surpassing the lateral resolution limit by a factor of two using structured illumination microscopy," J. Microsc. **198**, 82-87 (2000).
3. M. G. L. Gustafsson, "Nonlinear structured-illumination microscopy: Wide-field fluorescence imaging with theoretically unlimited resolution," Proc. Natl. Acad. Sci. **102**, 13081-13086, (2005).
4. G. Donnert, J. Keller, R. Medda, M. A. Andrei, S. O. Rizzoli, R. Lüthmann, R. Jahn, C. Eggeling, S. W. Hell, "Macromolecular-scale resolution in biological fluorescence microscopy," Proc. Natl. Acad. Soc. USA **103**, 11440-11445 (2006).
5. V. Westphal and S. W. Hell, "Nanoscale resolution in the focal plane of an optical microscope," Phys. Rev. Lett. **94**, 143903 (2005).
6. W. Lukosz and M. Marchant, "Optischen Abbildung Unter Ueberschreitung der Beugungsbedingten Aufloesungsgrenze," Opt. Acta **10**, 241-255 (1963).
7. W. Lucosz, "Optical Systems with Resolving Powers Exceeding the Classical Limit," J. Opt. Soc. Am. **57**, 932-941 (1967).
8. C. J. Schwarz, Y. Kuznetsova, and S. R. J. Brueck, "Imaging interferometric microscopy," Opt. Lett. **28**, 1424-1426 (2003).
9. S. A. Alexandrov T. R. Hillman, T. Gutzler and D. D. Sampson, "Synthetic aperture Fourier holographic optical microscopy," Phys. Rev. Lett. **97**, 168102 (2006).
10. V. Mico, Z. Zalevsky and J. Garcia, "Superresolution optical system by common-path interferometry," Opt. Express **14**, 5168-5177 (2006).
11. Y. Kuznetsova, A. Neumann, and S. R. J. Brueck, "Imaging interferometric microscopy – approaching the linear systems limits of optical resolution," Opt. Express **15**, 6651 (2007).
12. X. Chen and S. R. J. Brueck, "Imaging interferometric lithography - approaching the resolution limits of optics," Opt. Lett. **24**, 124-126 (1999).
13. Y. Kuznetsova, A. Neumann and S. R. J. Brueck, "Imaging interferometric microscopy," J Opt Soc Am A **25**, 811-822 (2008).
14. I. Tamaguchi, J. Kato, S. Ohta, and J. Mizuno, "Image formation in phase-shifting digital holography and applications to microscopy," Appl. Opt. **40**, 6177-6185 (2001).
15. T. Kreis, *Handbook of holographic interferometry: optical and digital methods* (Wiley-VCH Verlag GmbH & Co. KGaA, Weinheim, 2005).

1. Introduction

It is not necessary to explain the importance of resolution enhancement for millions of existing optical microscopes. The classical diffraction limit [1] has been successfully

exceeded in the impressive results of fluorescent microscopy [2-5]. However, there are many applications where non-fluorescent transmission/reflection microscopy is of critical importance. Much work has been reported in resolution improvement beyond the classic Rayleigh limit by synthetic aperture approaches [6-11].

We have previously demonstrated imaging interferometric microscopy (IIM) for the resolution enhancement of low numerical-aperture (NA) microscopes, using a Mach-Zehnder interferometer around the optical system, taking multiple offset partial images covering different regions of spatial frequency space, and synthesizing a complete image from these partial images [8, 11]. A related concept was first introduced for lithographic image formation (imaging interferometric lithography or IIL) [12]. Tilting the image plane in IIM allowed a close approach to the minimum theoretical linear systems resolution limit of $\sim \lambda/4$ (a maximum spatial frequency of $2/\lambda$) [11,13]. IIM requires building an interferometric system around the objective lens, and provides an optical solution to recording high spatial frequencies in the image plane.

In this paper we propose a new approach to achieve the same resolution using a simpler and more robust configuration. Structured illumination using two interfering illumination beams at different incident angles (an interferometer in the illumination system) provides an offset frequency coverage in which all of the image information is transmitted through the low- NA objective lens. The result is analogous to the intermediate frequency used in radio frequency communications, the recorded image information is at the low frequencies allowed by the objective lens. Procedures for extracting the image information and shifting it back to the true image high frequencies are described and demonstrated. Two major advantages of this approach are: a) because reduced or no access is required to the image pupil plane this approach is much more amenable to implementation on existing microscope systems, which typically do not offer image pupil plane access, and b) the recorded images are at low spatial frequencies which reduces demands on the resolution of the imaging camera (e. g. a smaller camera pixel count is sufficient as compared with the previous demonstrations). Another advantage of this method in comparison with conventional IIM is greater stability, due to the possibility of a much more compact interferometer, which no longer has to include the objective lens and other associated optics.

2. Structured Illumination

In previous papers we discussed conventional IIM with an extreme off-axis illumination beam (extreme is defined as illumination at an angle beyond the NA of the objective lens) and a coherent reference beam, equivalent to the zero-order transmission, reinjected into the objective lens Fourier plane using an optical fiber (Fig. 1(a)) [13]. As is easily seen, this is equivalent to constructing a Mach-Zehnder interferometer with one arm including the objective lens and requiring access to the image pupil plane. This can be difficult in an existing microscope system, where the pupil plane is not generally available and ancillary optics are required. In this paper, a second, coherent local-oscillator illumination beam at an offset angle just within the objective NA is introduced in addition to the extreme off-axis illumination to obtain the high frequency partial image (Fig. 1(b)). As seen in the figure, this results in building the interferometer in front of the object where there is more convenient access and smaller path lengths are possible. The interference between this local-oscillator beam and beams diffracted from the off-axis illumination beam and passing through the objective provide the high frequency information for the image. However, since the zero-order and the diffracted beams all pass through the low- NA objective, the image information is at low frequencies, $< 2NA/\lambda$, e.g. is in a shifted laboratory frame, and signal processing is necessary to restore the correct image frequencies. In addition, there are dark field terms arising from the interference between the diffracted orders from both illumination beams that must be eliminated. The optical and signal processing procedures necessary to achieve the final image are discussed below.

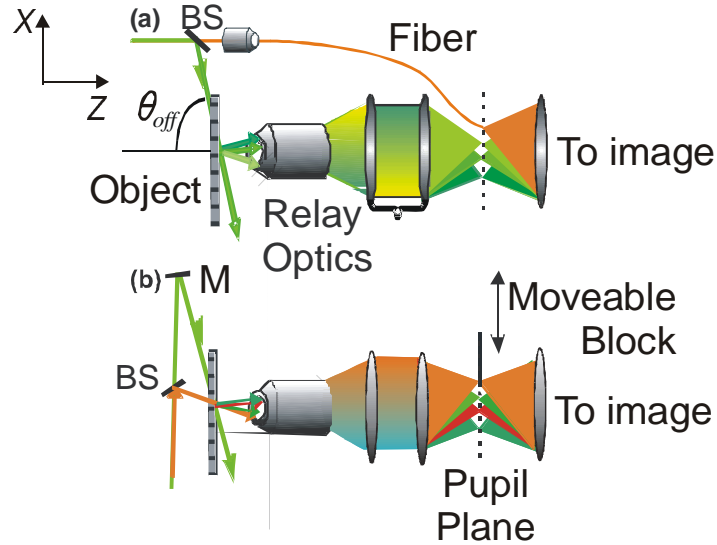


Fig. 1. Optical arrangements for (a) conventional IIM with an interferometer that includes the objective lens, and (b) structured illumination with the interferometer in front of the object.

We begin with a simple mathematical description, first of the extreme off-axis coherent illumination microscopy image of the previous IIM experiment (Fig. 1(a)) [13] and then extend this mathematical treatment to the present experiment. The total transmission through an arbitrary object illuminated by a tilted (off-axis) plane wave (assumed to be periodic on large scale to allow Fourier sums rather than Fourier integrals) and the optical system is given by:

$$A'_{0,0} \exp(-i\omega_{off}x) e^{i\gamma'_{0,0}z} + \sum_{k,l \neq 0} T(k\omega_x - \omega_{off}; l\omega_y) A_{k,l} \exp[ix(k\omega_x - \omega_{off}) + il\omega_y y] e^{i\gamma'_{k,l}z} \quad (1)$$

Where x , y and z are orthogonal spatial coordinates; $\omega_{off} = 2\pi \sin(\theta_{off})/\lambda$ is the spatial frequency offset arising from the off-axis illumination at angle θ_{off} (assumed in the x -direction), the prime on the $A'_{0,0}$ refers to the re-injected 0-order, ω_x , ω_y are the discrete spatial frequency increments of the Fourier summation; $\gamma'_{k,l} \equiv \left[(2\pi n/\lambda)^2 - (k\omega_x - \omega_{off})^2 - (l\omega_y)^2 \right]^{1/2}$ with n the refractive index of the transmission medium ($= 1$ for air); $\{k,l\}$ is the set of integers, for which $(\gamma'_{k,l})^2 > 0$, that is the range of integers for which the diffracted beams are within the band pass of the medium and are propagating in the z -direction, away from the object. A scalar electromagnetic model is adequate since the NA of the microscope system is relatively modest.

The transmission function of the optical system $T(k\omega_x; l\omega_y)$ is a simple band pass function:

$$T(k\omega_x; l\omega_y) = \begin{cases} 1 & \text{for } \sqrt{(k\omega_x)^2 + (l\omega_y)^2} \leq \omega_{MAX} = \frac{2\pi NA}{\lambda} \\ 0 & \text{else} \end{cases} \quad (2)$$

Taking the square of expression (1) provides the intensity on the imaging camera:

$$\begin{aligned}
& |A_{0,0}'|^2 + \dots\dots\dots(\text{dc offset}) \\
& \sum_{k,l \neq 0} A_{0,0}' A_{k,l}^* T(k\omega_x - \omega_{\text{off}}; l\omega_y) \exp[ik\omega_x x + il\omega_y y] e^{i(\gamma_{0,0}^{\text{off}} - \gamma_{k,l}^{\text{off}})z} + c.c. + \dots(\text{imaging}) \\
& \sum_{k,l \neq 0} \sum_{k',l' \neq 0} A_{k,l} T(k\omega_x - \omega_{\text{off}}; l\omega_y) A_{k',l'}^* T(k'\omega_x - \omega_{\text{off}}; l'\omega_y) \times \\
& \exp[i(k-k')\omega_x x + i(l-l')\omega_y y] e^{i(\gamma_{k,l}^{\text{off}} - \gamma_{k',l'}^{\text{off}})z} \dots\dots\dots(\text{dark field})
\end{aligned} \tag{3}$$

where the three terms on separate lines correspond to (top) a constant term, (middle) the imaging terms and (bottom) the dark field cross-correlation image. Subtracting out the dark field terms (by taking an image with the reference zero-order blocked so that only the third term survives) provides a sub-image that accurately captures the spatial frequency components that are transmitted through the optical system. Note that the imaging terms (middle line) are at the correct frequencies and that the offset illumination angle has cancelled out of the expression except for the filter transmission functions. Changing the illumination angle (and the angle of reintroduction) changes the offset allowing recording of a different region of frequency space.

Now consider structural illumination where there are two coherent illumination beams, one at the same offset as in the previous example (extreme off-axis, corresponding frequency shift denoted as ω_{off} and corresponding longitudinal wavenumber denoted as γ^{off}). The other beam come at the maximum offset allowed by the lens $\omega_{\text{offset}} \lesssim NA/\lambda$ denoted as ω_{NA} in the equation (and the corresponding γ^{NA}). Then the fields are:

$$\begin{aligned}
& A_{0,0} \exp(-i\omega_{\text{off}} x) e^{i\gamma_{0,0}^{\text{off}} z} + \sum_{k,l \neq 0} A_{k,l} \exp[i(k\omega_x - \omega_{\text{off}})x + il\omega_y y] e^{i\gamma_{k,l}^{\text{off}} z} + \\
& B_{0,0} \exp(-i\omega_{NA} x) e^{i\gamma_{0,0}^{NA} z} + \sum_{p,r \neq 0} B_{p,r} \exp[i(p\omega_x - \omega_{NA})x + ir\omega_y y] e^{i\gamma_{p,r}^{NA} z}
\end{aligned} \tag{4}$$

and squaring while taking advantage of the fact that the $A_{0,0}$ beam is not transmitted to the objective image plane while the $B_{0,0}$ beam is transmitted through the lens gives:

$$|B_{0,0}|^2 + \tag{5(a)}$$

$$\left\{ \sum_{p,r \neq 0} B_{0,0} B_{p,r}^* T(p\omega_x - \omega_{NA}; r\omega_y) \exp[i(p\omega_x x + r\omega_y y)] e^{i(\gamma_{0,0}^{NA} - \gamma_{p,r}^{NA})z} + c.c. + \right. \\
\left. \sum_{p,r \neq 0} \sum_{p',r' \neq 0} B_{p,r} B_{p',r'}^* T(p\omega_x - \omega_{NA}; r\omega_y) T(p'\omega_x - \omega_{NA}; r'\omega_y) \exp[i(p-p')x + i(r-r')y] e^{i(\gamma_{p,r}^{NA} - \gamma_{p',r'}^{NA})z} \right\} + \tag{5(b)}$$

$$\left\{ \sum_{k,l} B_{0,0} A_{k,l}^* T(l\omega_x - \omega_{\text{off}}; n\omega_y) \exp[-i(k\omega_x - \omega_{\text{off}} + \omega_{NA})x - ik\omega_y y] e^{i(\gamma_{0,0}^{NA} - \gamma_{k,l}^{\text{off}})z} + c.c. \right\} + \tag{5(c)}$$

$$\sum_{k,l} \sum_{k',l'} A_{k,l} A_{k',l'}^* T(k\omega_x - \omega_{\text{off}}; l\omega_y) T(k'\omega_x - \omega_{\text{off}}; l'\omega_y) \exp[i(k-k')\omega_x x + i(l-l')\omega_y y] e^{i(\gamma_{k,l}^{\text{off}} - \gamma_{k',l'}^{\text{off}})z} + c.c. \tag{5(d)}$$

$$\sum_{k,l} \sum_{p,r \neq 0} A_{k,l} B_{p,r}^* T(k\omega_x - \omega_{\text{off}}; l\omega_y) T(p\omega_x - \omega_{NA}; r\omega_y) \times \\
\exp[i(k-p)\omega_x + i(\omega_{NA} - \omega_{\text{off}})x + i(l-r)\omega_y] e^{i(\gamma_{k,l}^{\text{off}} - \gamma_{p,r}^{NA})z} + c.c. \tag{5(e)}$$

The first and the second (in the upper bracket) terms [(5a), (5b)] are just the result of the off-axis illumination at the edge of the pupil. This sub-image can be measured independently by blocking the extreme off axis beam, and subtracted from the sub-image. The third term (5c) is

the one we want, the image terms from the extreme off-axis illumination beating against a zero-order beam from the second illumination beam; because the zero-order beam is not at the correct angle to reset the frequencies to match the object frequencies (adjusted for magnification) there is a shift between the observed and the actual image plane frequencies that requires signal processing to reset (e.g. we are evaluating the Fourier components at an intermediate frequency). The fourth term (5d) is the dark field from the extreme off-axis illumination. Finally the last term (5e) is the combined dark field from the two illumination beams.

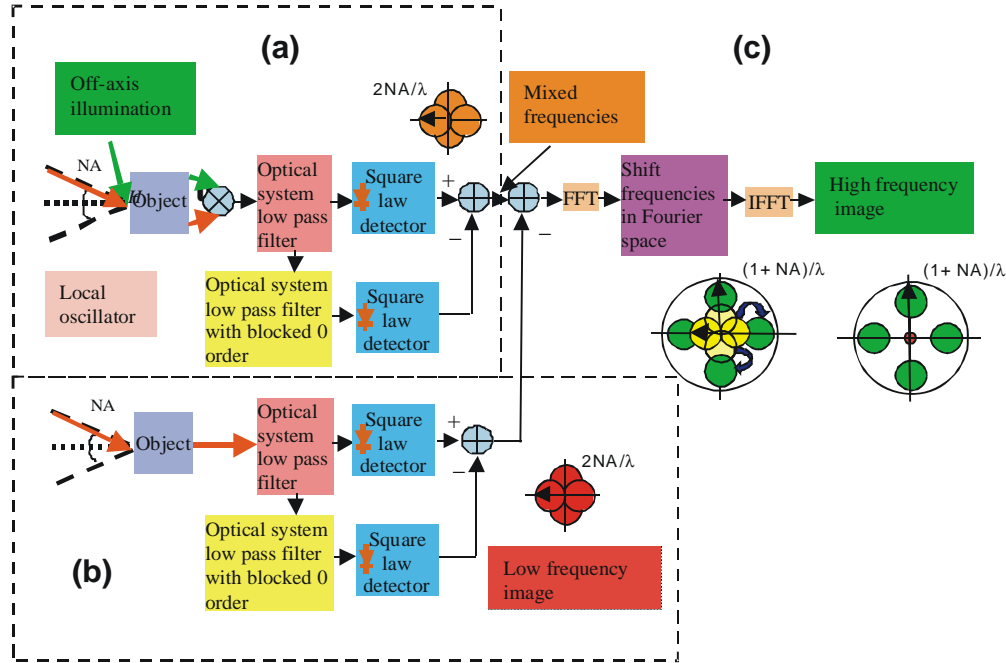


Fig. 2. Schematic of structural illumination and restoration algorithms: a) the object is illuminated simultaneously by two coherent beams: one at an extreme off-axis angle (green) and one (local oscillator, orange) at an angle of $\sim\sin^{-1}(NA)$ to the normal. High frequencies diffracted from the extreme off-axis illumination mix with low frequencies from the local oscillator, the dark field of the image is obtained by blocking the 0-order beam in the image pupil plane, b) low frequency image/dark field obtained by local oscillator illumination only with and without the 0-order blocked c) the dark field of the image is subtracted as well as the low frequency image without the dark field. Then frequencies are shifted in Fourier space and the total image can be reconstructed by standard IIM procedures: combining high and low frequency images.

Two approaches to eliminating the unwanted dark-field terms are presented. The first one requires blocking just the zero-order beam without making an obstacle to the other diffracted information. This can be done by adding a moveable block at the edge the objective pupil as shown in Fig. 1. A flow chart schematic of the procedure is shown in Fig. 2. The object is illuminated by two beams: one at an extreme off-axis angle (beyond the objective $\sin^{-1}(NA)$) and one (local oscillator) with an angle close to $\sin^{-1}(NA)$, such that its 0-order transmission is captured by the objective lens (Fig. 2(a)). By blocking only the 0-order we obtain the dark field image which can be subtracted from the image formed by interference of all of the orders from both beams [5(b), 5(d), and 5(e)]. Then we record the low frequency image obtained by the local oscillator object illumination with and without the 0-order blocked (Fig. 2(b)). We subtract the low frequency image without dark field from mixed image and restore high frequency image by shifting frequencies in Fourier space (Fig. 2(c)). The reconstructed image can be obtained by adding high frequency images with the low frequency images recorded in

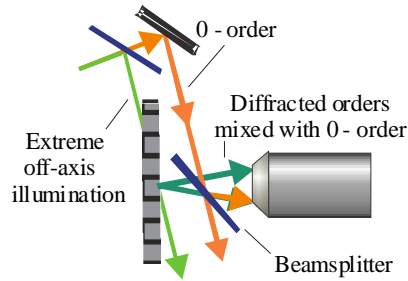


Fig. 3. Structured illumination with extreme off-axis illumination beam (green) and reference beam (orange) injected between object and objective lens.

necessary directions or just with on-axis illumination image as was done in the current experiment. This procedure is repeated in the orthogonal spatial direction for the Manhattan geometry test object; additional images are necessary for objects with arbitrary orientations. Appropriate filtering to deal with overlaps in frequency space coverage should be applied as has been discussed previously [13].

A second method to obtain the same result is to use a zero-order beam reinjected before the objective using a beamsplitter (Fig. 3). The beamsplitter is located between the object and the objective lens, eliminating all of the diffracted beams associated with the local oscillator, $B_{p,r} = 0, \forall p, r \neq 0$, and simplifying Eq. (5). We subtract the image dark field (recorded with blocked reference beam) and reference beam image (recorded with blocked illumination beam) using the same procedure described in Ref [8] and then restore high frequency image by shifting frequencies in Fourier space (Fig. 2).

Both methods have advantages and issues. The first arrangement requires access to the pupil plane of the system, which can be nontrivial. The second method does not contain the first, second and fifth terms ((5a), (5b), (5e)), so no access to the pupil plane is required, but it does require a beamsplitter between the object and the optical system which reduces the system working distance. Also, there is a possibility of introducing aberrations, especially if the beam splitter is at an angle to the optic axis; aberrations can be minimized by using a thin pellicle beamsplitter. In this configuration, it is particularly straightforward to use phase-shifting dark-field retrieval [14,15], as an alternative to blocking the reference zero-order, for eliminating the dark-field terms.

Interferometric methods require setting the phase relationship between the interferometer beams. This phase can be set in real time by observing the image of a reference object while adjusting the phase of one of the illumination beams. An alternative is to record images with an arbitrary phase shift and to evaluate the correct phase using signal processing approaches, again with the use of a reference object. MSE methods can be applied for higher precision in setting this phase. Even without the use of a reference object, the recorded image has higher contrast at the correct phase point, very analogous to the higher contrast observed in an image at focus, but this is a somewhat subjective evaluation and is certainly pattern dependent. The use of a reference object is a more reliable indicator of the correct phase.

3. Experimental results

For our experiments we use an $NA = 0.4$ objective with a He-Ne laser illumination source ($\lambda = 633$ nm) so that the Rayleigh resolution (above) is limited to ~ 950 nm. The results of a structural illumination experiment with 240 nm critical dimension (CD , equivalent to linewidth for these equal line:space structures) along with the corresponding simulations are shown in Fig. 4. The mixed image obtained as the result of the two-beam illumination and corresponding to the all terms of the Eq. (5) is shown in Figs. 4(a), 4(b); Figs. 4(c), 4(d) are

the images after subtraction of the dark field and low frequency image, and Figs. 4(e), 4(f) are restored high frequency images.

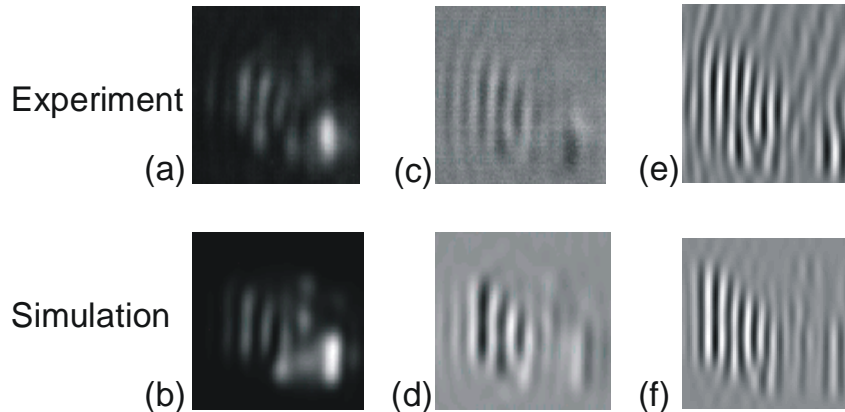


Fig. 4. (a,b) the mixed image corresponding to the interference of the low and high images, (c,d) the image after subtraction dark field and low frequency image, and (e,f) restored high frequency image.

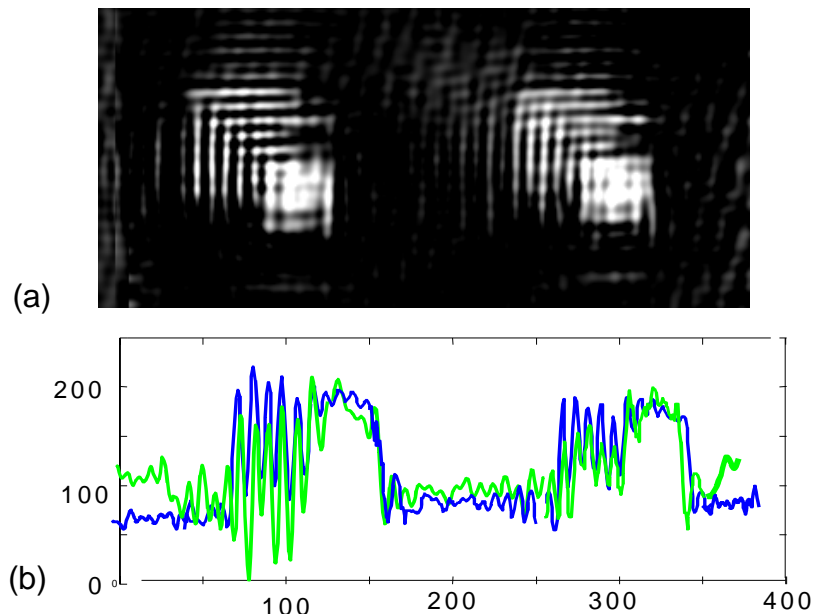


Fig. 5. (a). reconstructed image of 260- and 240-nm CD structures obtained using the optical configuration of Fig. 1 (b); (b) crosscut of the image (green) compared with a crosscut of corresponding simulation (blue).

The reconstructed image of 260- and 240-nm CD structures, within the same image field, obtained by this method is shown in Fig. 5(a). Figure 5(b) is a crosscut of the image through 260 nm 240 nm structures compared with a crosscut of the corresponding simulation. A total of four offset images, two each in the x - and y -directions, with $\theta_{ill} = 53^\circ$ and 80° were used along with a $0.4 NA$ objective. As discussed previously [13], this configuration provides resolution to $\lesssim 240$ nm CD. There is overlap in the frequency space coverage between these two exposures and frequency space filtering is used to assure a uniform coverage of frequency

space. The present Manhattan geometry structure has spectral content concentrated along the x - and y -directions, so the offset illuminations were restricted to those directions. It would be a simple matter to add additional frequency-space coverage for arbitrarily shaped structures by taking additional sub-images with rotation of the object around the (x,y) axes. The spatial frequency content of the image covers a wide range as a result of the large box (at 10X the linewidth of the line:space structures).

The reconstructed image of the same structures obtained by the method with the beamsplitter is shown in Fig. 6(a) and a crosscut of the image with corresponding simulation is shown in Fig. 6(b).

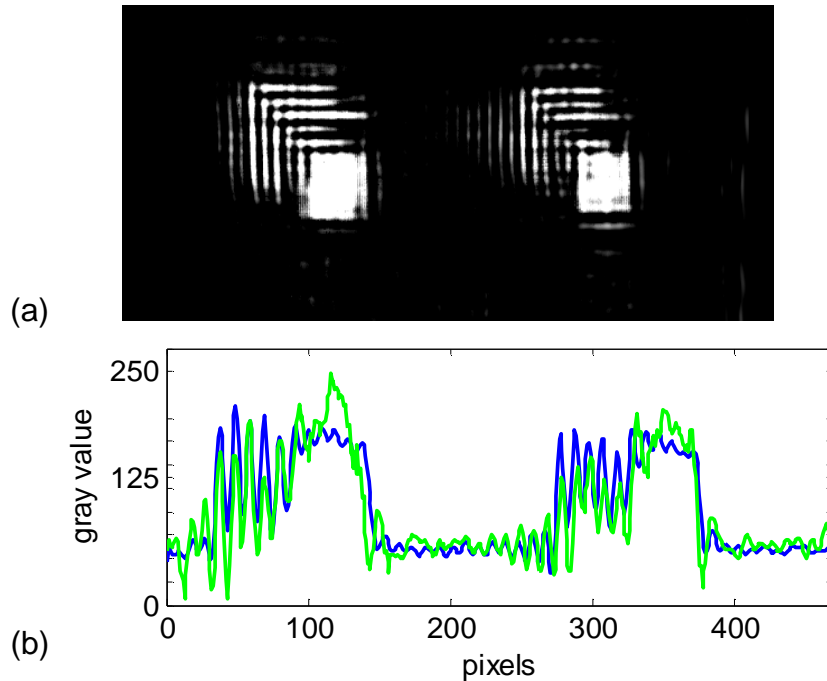


Fig. 6. (a). reconstructed image of 260- and 240-nm CD structures (reinjection of zero-order between object and objective lens (Fig. 3), b) crosscut of the image (green) compared with a crosscut of corresponding simulation (blue).

The quality of the experimental results for both methods is quite comparable. The first method retains a long working distance, but requires access to the imaging system pupil for blocking 0-order. The second does not require any modification to the traditional microscopy components, but has reduced working distance due to the beamsplitter in front of the objective.

There are some extra features experimentally as compared to the model due to the lack of precision in mutual phase determination between the sub-images and speckle effects from the coherent illumination. These issues can be reduced by using improved arrangements and lower coherence sources. There are other possible alternatives; the optimum choice will depend on the specifics of the object and the constraints of specific optical systems.

4. Conclusions

In the previous papers we demonstrated the possibility of increasing the resolution of an optical microscope with a low- NA objective, and demonstrated experimental results resolving a 240-nm CD Manhattan geometry (x, y pattern) object with a 0.4 NA objective at a wavelength of 633 nm ($R \sim \lambda/2.9$) without tilt of the object plane and of a 180-nm pattern ($R \sim$

$\lambda/3.52$) with tilt of the object plane. However, those results required the construction of a Mach-Zehnder interferometer around the lens which led to phase instability and difficulties in the adjustment. In addition, access to a relayed imaging-optical Fourier plane was required. Here we demonstrate alternative approaches to the same results by introducing the reference beam on the front side of the objective, including either a second off-axis illumination beam at an incident angle close to the edge of the imaging system NA or a reference beam, injected into the objective using a beamsplitter between the object and the objective lens. Both procedures require image restoration, since there is an offset in the frequencies necessarily associated with passing all of the beams through the low-pass filter of the objective lens NA . The first technique retains the long working distance of the low- NA lens, but requires access to the illumination system pupil. The method with a beamsplitter between the object and the objective lens does not require this access but has shortened working distance as a result of accommodating the beamsplitter. In both cases, extension to the tilted object case is straightforward, so that the resolution extends to $\sim \lambda/4$ and to $\sim \lambda/4n$ with immersion. The demonstrated techniques require only a minimal access to the microscope system which makes them much more adaptable to current technology. Specific application areas of interest include semiconductor manufacturing metrology and biosensors.

Acknowledgments

We are grateful to Felix Jaeckel for e-beam writing of the mask with small features. Support for this work was provided by DARPA under the University Photonics Research Center Program.